

X-Ray Spectroscopy of Newly Identified ULXs Associated With M87’s Globular Cluster Population

Kristen C. Dage,^{1*} Stephen E. Zepf,¹ Erica Thygesen,¹ Arash Bahramian,²
Arunav Kundu,³ Thomas J. Maccarone,⁴ Mark B. Peacock,¹ Jay Strader¹

¹*Department of Physics and Astronomy, Michigan State University, East Lansing, MI 48824*

²*International Centre for Radio Astronomy Research – Curtin University, GPO Box U1987, Perth, WA 6845, Australia*

³*Eureka Scientific, Inc., 2452 Delmer Street, Suite 100 Oakland, CA 94602, USA*

⁴*Department of Physics, Box 41051, Science Building, Texas Tech University, Lubbock, TX 79409-1051, USA*

Accepted XXX. Received YYY; in original form ZZZ

ABSTRACT

We have identified seven ultraluminous X-ray sources (ULXs) which are coincident with globular cluster candidates (GCs) associated with M87. ULXs in the old GC environment represent a new population of ULXs, and ones likely to be black holes. In this study we perform detailed X-ray spectroscopic followup to seven GC ULXs across a wealth of archival *Chandra* observations and long time baseline of 16 years. This study brings the total known sample of GC ULXs to 17. Two of these sources show variability in their X-ray luminosity of an order of magnitude over many years, and one of these sources shows intra-observational variability on the scale of hours. While the X-ray spectra of the majority of globular cluster ULXs are best fit by single component models, one of the sources studied in this paper is the second GC ULX to be best fit by a two component model. We compare this new sample of GC ULXs to the previously studied sample, and compare the X-ray and optical properties counterparts across the samples. We find that the clusters that host ULXs in M87 have metallicities from $g - z = 1.01$ to $g - z = 1.70$. The best-fit power-law indices of the X-ray spectra range from $\Gamma = 1.37 - 2.21$, and the best fit inner black-body disk temperatures range from $kT = 0.56 - 1.90$ keV.

Key words: M87: globular clusters: general – stars: black holes – X-rays: binaries

1 INTRODUCTION

M87 is an elliptical galaxy in the Virgo group, and home to thousands upon thousands of globular clusters (GCs) (Harris 2009). While M87 is best known for hosting a super massive black hole with high energy jets, the galaxy is filled with hot gas with energies up to 2.5keV (e.g. Fabricant et al. 1978). This hot gas makes studying fainter source populations difficult, but the brightest X-ray sources can be readily found and studied above the background from the hot gas.

The brightest X-ray sources are known as ultraluminous X-ray sources (ULXs) and are sources which typically exceed $\sim 10^{39}$ erg/s (i.e. above the Eddington limit for a $10 M_{\odot}$ black hole) (Fabbiano & White 2006). These sources are thought to be a \sim stellar mass compact object plus a donor star accreting in a different regime of physics than typical X-ray binaries.

Kajava & Poutanen (2009) show that there are likely to be at least two classes of ULXs observed within the young star-forming galaxies. One class is ULXs that are persistently below 3×10^{39} erg/s

that show relatively hot thermal spectra where the source variations are consistent with $L \propto T^4$. The other set of sources shows power law dominated spectra, and a quasi-thermal soft excess (e.g., Walton et al. 2018).

Many ULXs have massive donor stars (e.g., Gladstone et al. 2013), and the majority of them have been found associated with the star-forming regions of galaxies (e.g., Brightman et al. 2019, and references therein). Of the ULXs identified in star-forming regions of galaxies, six have had a neutron star (NS) identified as the primary accretor in the system via detection of pulsations, and many more systems like this are thought to also be powered by a NS (Song et al. 2020; Jithesh et al. 2020), which is perhaps highly magnetized and/or beamed (King 2008; Brightman et al. 2018). However, ten sources with ultraluminous X-ray luminosities that were bright on the scale of years have been found to be associated with globular clusters (GCs) in nearby elliptical galaxies, (Maccarone et al. 2007; Irwin et al. 2010; Shih et al. 2010; Maccarone et al. 2011; Roberts et al. 2012; Dage et al. 2019a), as well as two GC sources which flared to above 10^{39} erg/s on the timescale of minutes (Irwin et al. 2016). As old stellar populations, GCs are not home to the types of massive donor stars typically associated with ULXs, and the

* E-mail: kcdage@msu.edu

ULXs associated with the two types of galaxies are likely distinct populations (e.g. [Irwin et al. 2003](#)). At least one GC ULX is likely to be a black hole (BH) accreting off of a white dwarf (see [Zepf et al. 2008](#); [Steele et al. 2011](#); [Peacock et al. 2012](#); [Dage et al. 2019b](#) and references therein).

A systematic study of the known GC ULXs by [Dage et al. 2019a](#) revealed that sources were either best fit by a power-law model, or by black-body disk model. The accretion disk models fits fell into one of two groups: either the sources were better fit by a higher disk temperature or had a lower disk temperature with the spectral parameter constant while varying in luminosity. There is a likely correlation between the disk temperature and whether or not the source has optical emission, as the optical spectra of the low temperature sources show forbidden optical emission lines beyond the globular cluster continuum, and a number of the higher temperature sources have no emission beyond the cluster continuum ([Dage et al. 2019a](#)). However, this conclusion is tentative because the number of GC ULXs is still small.

Understanding the number and nature of these rare sources has implications not just for accretion physics, but for addressing the question of black holes in extragalactic globular clusters. While black holes (or good black hole candidates) have begun to be observed in Galactic globular clusters (see [Strader et al. 2012](#); [Chomiuk et al. 2013](#); [Miller-Jones et al. 2015](#); [Giesers et al. 2018](#); [Shishkovsky et al. 2018](#); [Giesers et al. 2019](#) for recent examples), the methods used to detect quiescent BHs in Galactic GCs cannot be used to search for BHs in extragalactic GCs. Thus, searching for ULXs in extragalactic GCs is the best option for identifying BH candidates in GCs outside our own Galaxy.

One very likely scenario to form at least some black hole-black hole binaries (BBHs) are GCs ([Abbott et al. 2016](#); [Rodriguez et al. 2019](#)). Clusters represent an older population of stars, which will have initially produced many BHs. Because of the dynamic environment, the cross section for interaction is high and binaries can form easily. Once formed, BHs may possibly drive the cluster evolution ([Giersz et al. 2019](#); [Kremer et al. 2019](#)). Observational studies of BHs in GCs have a large impact both on understanding cluster evolution, as well as giving clues to the conditions that BBHs form in. ULX sources in GCs offer a complementary path to help answer the question of numbers of BHs in GCs, as well as touch on the question of the origins of the progenitors of LIGO sources.

In this body of work, we use *Chandra* observations of M87 and its surrounding regions to identify ultraluminous X-ray sources coincident with GCs. The observations and analysis are laid out in Section 2, major results are highlighted in Section 3, and the implications of this work are discussed in Section 4.

2 OBSERVATIONS AND ANALYSIS

M87 has a wealth of archival data available, including 28 *Chandra* ACIS observations with the duration of 15 ks or longer (see Table 1). M87 is host to almost 15,000 globular clusters, and we utilize the photometric globular cluster catalogs which have conservatively modeled and removed contaminant populations from [Oldham & Auger 2016](#) as well as catalogs of confirmed globular clusters ([Strader et al. 2011](#); [Caldwell et al. 2014](#)).

2.1 Identification of Globular Cluster ULXs

We reprocessed the *Chandra* data using CIAO version 4.11 ([Fruscione et al. 2006](#)) `chandra_repro` and CalDB version 4.10. We

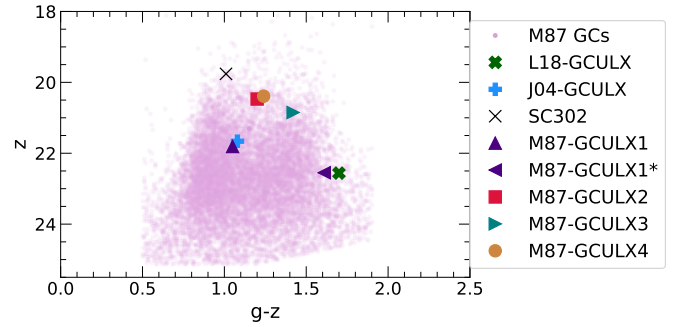


Figure 1. z versus $g - z$ for M87 globular cluster photometric candidates from [Jordán et al. 2009](#); [Oldham & Auger 2016](#), with color and magnitude of GC candidates hosting ULXs plotted overtop.

filtered out any background flares. We used the `Wavdetect` function within CIAO to identify X-ray point sources across the observations using 0.5-7.0 keV images. We used an exposure map centered at 2.3 keV, and wavelet scales at 1.0, 2.0, 4.0, 8.0 and 16.0 pixels. Once the images had been cleaned and filtered, we ran `wavdetect` using an enclosed count fraction (e.c.f.) of 0.3¹ and significance threshold of 10^{-6} which corresponds to about one false detection per chip. We then used the `srcflux` function to estimate unabsorbed X-ray fluxes assuming a fixed Galactic line of sight N_H of 2.54×10^{20} cm^{-2} ([Dickey & Lockman 1990](#)) and a fixed power-law index of $\Gamma = 1.7$, which is the typical power-law index for X-ray binaries.

The X-ray luminosity of the sources was estimated using a distance of 16.8 Mpc ([Macri et al. 1999](#)), and selected sources which reached an estimated X-ray luminosity of 7×10^{38} erg/s or above (as using a fixed model tends to underestimate the flux slightly) at one point during the observations. This allowed us to be sensitive to transient ULX sources which may have only brightened once during the sequence of observations, as well as persistent ones. We used TOPCAT ([Taylor 2005](#)) to match the globular cluster catalogs ([Jordán et al. 2009](#); [Oldham & Auger 2016](#)) to the ULX sources with a 0''.8 tolerance². This provided us with a sample of seven ULXs overlapping with globular cluster candidates (Table 2 and Figure 1). Several of these sources were also identified in [Jordán et al. 2004](#); [Luan et al. 2018](#). One of these sources is located in the Virgo cold front ($\sim 19'$ from the galaxy center) and another is located in a field $\sim 8'$ from the galaxy center. The remaining five sources are near the galaxy center. The closest source to the active jet region is $\sim 6''.8$ away, and the farthest source $\sim 130''$ from the centre (see Figure 2). A comparison of the host clusters colors and z -magnitudes (de-reddened³) to other clusters in M87 are plotted in Figure 1.

2.2 X-ray Spectroscopy

Once the seven GC ULXs were identified, we extracted the source spectra in every observation that had a point source associated with the source's position using CIAO with 1.2'' circular source extraction regions, with a series of similar sized region files placed around

¹ We chose a low value because of the high background.

² 0''.8 is the 90% uncertainty radius of *Chandra*'s absolute astrometry: <https://cxc.harvard.edu/cal/ASPECT/celmon/>

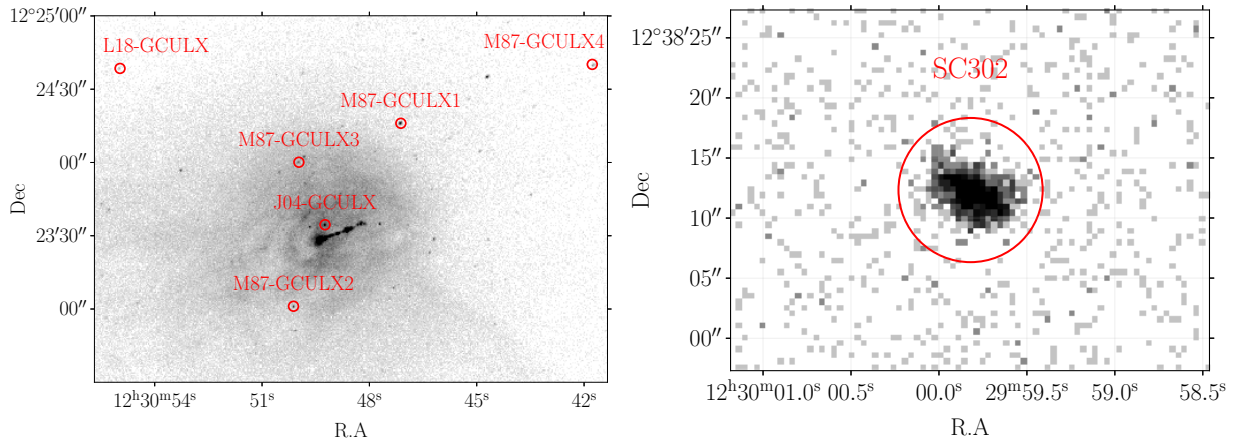
³ <https://irsa.ipac.caltech.edu/cgi-bin/bgTools/nph-bgExec>

Table 1. Chandra observations of M87 with observations greater than 15 ks. All are ACIS-S with no grating unless indicated otherwise.

ObsID	Date	Exposure (ks)	Sources in FOV	ObsID	Date	Exposure (ks)	Sources in FOV
241 (HETG)	2000-07-17	40.0	1	15180 (ACIS-I)	2013-08-01	140.0	SC302
352	2000-07-29	40.0	L18, J04, 1-4	16585 (ACIS-I)	2014-02-19	45.0	SC302
2707	2002-07-06	105.0	L18, J04, 1-4	16586 (ACIS-I)	2014-02-20	50.0	SC302
3717	2002-07-05	23.0	L18, J04, 1-3	16587 (ACIS-I)	2014-02-22	38.0	SC302
4007	2003-11-21	40.0	None	16590 (ACIS-I)	2014-02-27	38.0	SC302
5826 (ACIS-I)	2005-03-03	140.0	L18, J04, 1-4	16591 (ACIS-I)	2014-02-27	24.0	SC302
5827 (ACIS-I)	2005-05-05	160.0	L18, J04, 1-4	16592 (ACIS-I)	2014-03-01	36.0	SC302
5828 (ACIS-I)	2005-11-17	33.0	L18, J04, 1-4	16593 (ACIS-I)	2014-03-02	38.0	SC302
6186 (ACIS-I)	2005-01-31	48.0	L18, J04, 1-3	18781	2016-02-24	45.0	J04, 1-3
7210 (ACIS-I)	2005-11-16	32.0	L18, J04, 1, 3,4	18782	2016-02-26	37.0	J04, 1-3
7211 (ACIS-I)	2005-11-16	17.0	L18, J04, 1-3	18783	2016-04-20	40.0	J04, 2,3
11783	2010-04-13	30.0	L18	18836	2016-04-28	43.0	J04, 2,3
15178 (ACIS-I)	2014-02-17	47.0	SC302	18838	2016-05-28	62.0	J04, 2,3
15179 (ACIS-I)	2014-02-24	44.0	SC302	18856	2016-06-12	28.0	J04, 2,3

Table 2. RA and Dec of identified GC ULXs within M87's system. Photometric values (de-reddened z-band magnitude and g-z color) from [Jordán et al. 2009](#); [Oldham & Auger 2016](#), Strader et al in prep. Sources marked with * are found in Strader et al in prep., ^o from [Oldham & Auger 2016](#), and † were identified in ([Jordán et al. 2009](#)). r_h values are from [Jordán et al. 2009](#) or measured from HST data using lshape. M87-GCULX1 was matched to two clusters and we present values for both cluster parameters ([Larsen 1999](#)).

Name	RA	Dec	z-band (AB mag)	g-z (AB mag)	r_h (pc)	L_X ($\times 10^{39}$ erg/s)
CXOU J122959.82+123812.33 (SC302) *	12:29:59.82	+12:38:12.33	19.76	1.01	-	1.65
CXOU J123054.97+122438.51 (L18-GCULX) †	12:30:54.97	+12:24:38.51	22.56	1.70	1.88	1.05
CXOU J123049.24+122334.52 (J04-GCULX) †	12:30:49.24	+12:23:34.52	21.66	1.08	2.20	0.80
CXOU J123047.12+122416.06 (M87-GCULX1) ^o †	12:30:47.12	+12:24:16.06	21.73/22.55	1.05/1.61	3.69/1.96	1.64
CXOU J123050.12+122301.14 (M87-GCULX2) ^o †	12:30:50.12	+12:23:01.14	20.47	1.29	1.82	1.01
CXOU J123049.97+122400.11 (M87-GCULX3) ^o †	12:30:49.97	+12:24:00.11	20.85	1.42	2.53	1.14
CXOU J123041.77+122440.16 (M87-GCULX4) ^o	12:30:41.77	+12:24:40.16	20.41	1.24	2.70	1.08


Figure 2. *Left* - 0.5-7.0 keV band image of M87 (from ObsID 2707) and four of the ULXs identified and studied in this work. *Right* - X-ray 0.5-7.0 keV band images of SC302 (ObsID 15180). This source is observed at high ($> 4'$) off-axis angles, thus shows non-circular point spread functions.

the source to extract background spectra, taking care to avoid any neighbouring X-ray sources.

After extracting all spectra, we used COMBINE_SPECTRA to combine the spectra, and binned by 20 using DMGROUP to have one deep spectrum for every source. Previous studies of GC ULXs have established that they are fit well either by an absorbed multi-colored disk (tbabs*diskbb in Xspec; e.g., [Mitsuda et al. 1984](#)) and/or an absorbed power-law (tbabs*pegpwr1w in Xspec;

e.g., [Irwin et al. 2010](#); [Shih et al. 2010](#); [Maccarone et al. 2011](#); [Roberts et al. 2012](#)), or an additive combination of the two models (tbabs*(diskbb+pegpwr1w) in Xspec; e.g., [Maccarone et al. 2007](#)). We used these models to fit the combined spectra of the

sources in our sample of GC ULXs in M87 and used F-Test⁴ to determine if the two-component model was likely to be a better fit. Fit results and statistics (for combined spectra) are presented in Table 3. We also considered effects of a secondary absorption column in each source. However we found that in all cases this second column is consistent with zero and thus used a single absorption column.

We also performed spectral analysis on the individual observations for each source, modeling extracted spectra with `tbabs*diskbb` and `tbabs*pegpwr1w`. Any source spectrum with ≥ 100 counts was binned by 20 events per bin. For source spectra with less than 100 counts, we binned them by 1 count per bin and fit the same models using W-statistics (Cash 1979). J04-GCULX, M87-GCULX2 and M87-GCULX3 were especially challenging to fit in X-ray due to their proximity to the center of the jet, and the high background. All individual spectra of M87GCULX3 were entirely fit with W-statistics.

The results of our spectral analysis and the best-fit values for each of the sources are presented in Tables 4-10.

Among the two sources farther away from the galaxy, SC302 was well monitored over a short period of time in the Virgo Cold Front (ObsIDs 15178-16593).

M87-GCULX4 was not in any observation after ObsID 7210 because it was off the chip for the remainder of the observations. We used PIMMS to estimate upper limits for M87-GCULX3 in ObsID 352, and for M87-GCULX2 in ObsID 18783, using the value of the best fit power-law index from the longest observation. The upper limit flux estimates based on the count rates are included in Table 11, as well as Tables 4-10.

2.3 X-Ray Variability

We searched for intra-observational variability by extracting background subtracted source lightcurves using CIAO's `dmextract` in the longest observations of the sources (over 100ks per observation). The majority of the sources revealed no clear intra-observational variability. Two of these sources, J04-GCULX and M87-GCULX1 were also studied by Foster et al. 2013, and showed no periodic variability on the scale of weeks to years.

The lightcurves of the majority of these sources also showed no clear short-term changes on the scale of hours (these lightcurves are plotted in Appendix A). The exception to this is SC302, which showed strong intra-observational variability in some (but not all) of the extracted light curves. We extracted the light curves from all observations of this source (Figure 3).

We used FTOOLS `lcstats`⁵ to quantify the variability in each of the observations, and found that the RMS fractional variation of every observation was a 3σ upper limit, with the exception of SC302 during four observations. These values are presented in Table 12.

3 RESULTS

Using the wealth of archival *Chandra* data available for M87 and its outlying regions, we identified 7 ultraluminous X-ray sources which are associated with M87's globular clusters. Of these, one cluster (SC302) is spectroscopically confirmed (matched to Strader et al

in prep, see also Caldwell et al. 2014) and the rest are photometric GC candidates (matched to sources from catalogs from Jordán et al. 2004; Oldham & Auger 2016).

We extracted and fit the X-ray spectra of these sources across ~ 16 years worth of extant data, using a single absorbed power-law model and a single absorbed black-body disk model. We cannot differentiate between the models for the sources over most of the observations, as most of the sources had a similar $\chi^2/\text{d.o.f.}$ to each other for each model. SC302 and M87-GCULX1 were better fit by an absorbed multi-colored disk and an absorbed power-law respectively for some observations, and equally well in the rest.

3.1 Power-Law Model Fits

The best fit power-law indices of the sources in the M87 sample have been plotted against their unabsorbed X-ray luminosities in Figure 4, along with the same values for the previously studied GC ULXs in Dage et al. 2019a. To evaluate any potential correlations between X-ray luminosity (in log scale) and power-law photon index or disk blackbody inner temperature, we used Pearson's r and Spearman's rank. We note that all data points have non-negligible uncertainties. Thus, we used bootstrap sampling (random draws for each data point based on the uncertainties) and calculated correlation coefficient for each randomized sample and evaluated the significance of correlation for each source based on the final distribution of correlation coefficients. We found that there is no statistical evidence for clear correlation between the best-fit X-ray parameters and the X-ray luminosity, except perhaps a $\sim 1\sigma$ suggestion of correlation in M87-GCULX3. These sources seem to show a similar clustering to the previously studied sources, except for GCU8 in NGC 1399, which appears to be much brighter and harder than the rest of the sample. J04-GCULX shows an interestingly wide range of best fit power-law indices.

3.2 Blackbody Disk Model Fits

In Figure 5, we plot the best fit inner disk temperature (kT_{in}) for each observation versus the corresponding X-ray luminosity, with the same values for the larger GC ULX population plotted in the background for comparison. None of the M87 GC ULX sources appear to behave like GCU7 in NGC 1399 or RZ2109 in NGC 4472, which have very self-consistent values kT_{in} and a wide range of luminosities, which highlights how rare these two sources are.

3.3 Short and Long Term-X-Ray Variability of Sources

Lightcurves from this study, as well as the sources in Dage et al. 2019a suggest that GC ULXs do not typically vary within an observation. RZ2109 (Maccarone et al. 2007), the GC ULX in NGC 1399 which faded below the detection limit of any subsequent observations after 2003 (Shih et al. 2010), and now SC302 seem to be the exceptions to this rule with their strong intra-observational variability.

Figure 6 shows the best fit unabsorbed X-ray luminosity values for each source versus the MJD of the observation, along with upper limits. SC302 does not appear to vary greatly in L_X across observations, which is interesting because the source appears to vary within a factor of two during some observations. SC302's long-term variability was only probed over the course of around a year, and further monitoring could reveal interesting long-term variability. It is of note that none of these sources rose above 4×10^{39}

⁴ <https://heasarc.gsfc.nasa.gov/xanadu/xspec/manual/node83.html>

⁵ <https://heasarc.gsfc.nasa.gov/docs/xanadu/xronos/help/lcstats.html>

Table 3. Single component model fits to the stacked spectra of M87’s GC ULXs, with the F-Test comparison to the two component models for the best single-component model tabulated below (lower F-test probability indicates a higher likelihood that adding a second component improves the fit). Γ_{PL} represent power-law photon index, kT_{in} is the inner disk temperature in the disk blackbody model, χ^2_{ν} indicates reduced χ^2 , and d.o.f. stands for degrees of freedom in the fit.

Source	power-law			diskbb		
	Γ_{PL}	$\chi^2_{\nu}/\text{d.o.f.}$	F-Test prob. (%)	kT_{in} (keV)	$\chi^2_{\nu}/\text{d.o.f.}$	F-Test prob. (%)
SC302	2.07 (\pm 0.05)	2.00/110	–	0.92 (\pm 0.04)	0.98/110	0.8
L18-GCULX	2.03 (\pm 0.11)	1.11/96	–	0.81 (\pm 0.09)	1.03/96	1.5
J04-GCULX	2.21 (\pm 0.09)	1.06/147	1.4	0.74 (\pm 0.07)	1.26/147	–
M87-GCULX1	2.17 (\pm 0.05)	1.35/120	\ll 0.01	0.67 (\pm 0.04)	1.39/120	–
M87-GCULX2	1.52 (\pm 0.11)	1.00/106	–	1.44 (\pm 0.21)	0.95/106	20.6
M87-GCULX3	1.36 (\pm 0.09)	0.91/117	7.7	1.90 (\pm 0.28)	0.94/117	–
M87-GCULX4	1.37 (\pm 0.15)	1.02/44	23.8	1.86 ($^{+0.56}_{-0.38}$)	1.36/44	–

Table 4. *Chandra* Fit Parameters and Fluxes (0.5-8 keV) for spectral best fit single-component models, `tbabs*pegpwlw` and `tbabs*diskbb` for SC302. Hydrogen column density (N_H) frozen to $2.54 \times 10^{20} \text{cm}^{-2}$. All fluxes shown are unabsorbed in the 0.5-8keV band.

SC302							
ObsID (Date)	TBABS*PEGPWLW			TBABS*DISKBB			
	Γ	$\chi^2_{\nu}/\text{d.o.f.}$	PL Flux ($10^{-14} \text{erg s}^{-1} \text{cm}^{-2}$)	T_{in} (keV)	Disk Norm (10^{-3})	$\chi^2_{\nu}/\text{d.o.f.}$	Disk Flux ($10^{-14} \text{erg s}^{-1} \text{cm}^{-2}$)
15178 (2014-02-17)	2.1 (\pm 0.3)	1.32/7	6.6 (\pm 0.9)	0.9 ($^{+0.2}_{-0.1}$)	4.5 ($^{+4.7}_{-2.3}$)	1.19/7	5.0 (\pm 0.7)
15179 (2014-02-24)	2.1 (\pm 0.3)	2.25/9	9.1 (\pm 1.1)	0.8 (\pm 0.1)	8.7 ($^{+6.9}_{-3.9}$)	1.35/9	7.0 (\pm 0.7)
15180 (2013-08-01)	2.0 (\pm 0.1)	1.57/53	11.3 (\pm 0.1)	1.0 (\pm 0.1)	4.9 (\pm 1.1)	0.83/53	9.9 (\pm 0.6)
16585 (2014-02-19)	2.1 (\pm 0.3)	1.19/6	6.8 (\pm 1.0)	0.8 (\pm 0.2)	8.3 ($^{+8.9}_{-6.5}$)	0.29/6	4.9 (\pm 0.7)
16586 (2014-02-20)	1.9 (\pm 0.5)	0.57/6	7.4 (\pm 1.5)	0.8 ($^{+0.3}_{-0.2}$)	\leq 6.8	0.73/6	4.9 ($^{+1.1}_{-8.0}$)
16587 (2014-02-22)	2.1 (\pm 0.4)	1.64/6	7.3 (\pm 1.1)	0.9 ($^{+0.3}_{-0.2}$)	4.5 ($^{+6.5}_{-2.7}$)	1.92/6	5.4 (\pm 0.9)
16590 (2014-02-27)	1.9 (\pm 0.3)	1.23/5	6.6 (\pm 1.0)	1.0 ($^{+0.3}_{-0.2}$)	2.4 ($^{+3.2}_{-1.5}$)	1.10/5	5.1 (\pm 0.9)
16591 (2014-02-27)	2.1 (\pm 0.9)	0.22/2	8.4 ($^{+3.9}_{-1.7}$)	0.7 ($^{+0.8}_{-0.3}$)	\leq 11.9	0.55/2	5.5 ($^{+2.9}_{-1.1}$)
16592 (2014-03-01)	1.7 (\pm 0.5)	0.42/4	7.9 ($^{+2.0}_{-1.5}$)	1.0 ($^{+0.3}_{-0.2}$)	\leq 2.6	0.23/4	5.5 ($^{+1.6}_{-1.1}$)
16593 (2014-03-02)	1.9 ($^{+0.5}_{-0.4}$)	0.63/4	6.6 ($^{+1.4}_{-1.1}$)	1.0 ($^{+0.4}_{-0.3}$)	\leq 2.9	1.03/4	4.7 ($^{+1.2}_{-0.5}$)

Table 5. *Chandra* Fit Parameters and Fluxes (0.5-8 keV) for spectral best fit single-component models, `tbabs*pegpwlw` and `tbabs*diskbb` for L18-GCULX. Hydrogen column density (N_H) frozen to $2.54 \times 10^{20} \text{cm}^{-2}$. Lower count observations fit with W-stat have their statistics presented in parentheses. All fluxes shown are unabsorbed. Values marked with † are upper-limits based on the count rate of a non-detection (see Table 11), values marked with - were detections but could not be fit with the `diskbb` model.

L18-GCULX							
ObsID (Date)	TBABS*PEGPWLW			TBABS*DISKBB			
	Γ	$\chi^2_{\nu}/\text{d.o.f.}$ or (W-stat)	PL Flux ($10^{-14} \text{erg s}^{-1} \text{cm}^{-2}$)	T_{in} (keV)	Disk Norm (10^{-3})	$\chi^2_{\nu}/\text{d.o.f.}$ or (W-stat)	Disk Flux ($10^{-14} \text{erg s}^{-1} \text{cm}^{-2}$)
352 (2000-07-29)†	†	\leq 2.1	†	†	†	†	†
2707 (2002-07-06)	2.79 ($^{+1.6}_{-1.0}$)	1.4 ($^{+0.9}_{-0.6}$)	(148.79/172)	0.7 ($^{+0.6}_{-0.4}$)	\leq 1.8	(149.62/172)	0.9 ($^{+0.4}_{-0.4}$)
3717 (2002-07-05)†	†	\leq 2.0	†	†	†	†	†
5826 (2005-03-03)	1.7 (\pm 0.3)	1.09/22	5.5 (\pm 1.1)	1.1 ($^{+0.4}_{-0.3}$)	1.5 ($^{+2.3}_{-1.0}$)	1.03/33	2.3 (\pm 1.0)
5827 (2005-05-05)	2.5 (\pm 0.3)	1.29/33	2.2 (\pm 0.3)	0.5 ($^{+0.2}_{-0.1}$)	20.1 ($^{+46.0}_{-14.5}$)	1.52/33	1.6 (\pm 0.3)
5828 (2005-11-17)	2.0 ($^{+0.6}_{-0.5}$)	(82.55/90)	6.7 (\pm 0.8)	0.6 ($^{+0.6}_{-0.2}$)	\leq 5.3	(83.00/90)	1.6 ($^{+0.8}_{-0.6}$)
6186 (2005-01-31)	2.1 (\pm 0.2)	1.61/16	1.7 (\pm 0.9)	0.8 (\pm 0.1)	7.7 ($^{+7.0}_{-3.6}$)	1.48/16	5.1 (\pm 0.7)
7210 (2005-11-16)	2.5 ($^{+1.1}_{-0.9}$)	0.26/4	3.0 ($^{+0.4}_{-0.2}$)	0.5 ($^{+0.4}_{-0.2}$)	\leq 16.7	0.25/4	2.0 (\pm 0.6)
7211 (2005-11-16)	2.1 (\pm 0.4)	(56.59/56)	5.0 ($^{+1.3}_{-1.1}$)	0.8 ($^{+0.3}_{-0.2}$)	5.1 ($^{+8.6}_{-3.4}$)	(52.40/56)	4.0 ($^{+1.0}_{-0.8}$)
11783 (2010-04-13)†	†	†	\leq 1.0	†	†	†	†

Table 6. *Chandra* Fit Parameters and Fluxes (0.5–8 keV) for spectral best fit single-component models, `tbabs*pegpwlw` and `tbabs*diskbb` for J04-GCULX. Hydrogen column density (N_H) frozen to $2.54 \times 10^{20} \text{cm}^{-2}$. Lower count observations fit with W-stat have their statistics presented in parentheses. All fluxes shown are unabsorbed. Values marked with † are upper-limits based on the count rate of a non-detection (see Table 11), values marked with - were detections but could not be fit with the `diskbb` model.

J04-GCULX							
ObsID (Date)	TBABS*PEGPWLW			TBABS*DISKBB			
	Γ	χ^2_{ν} /d.o.f. or (W-stat)	PL Flux ($10^{-14} \text{ erg s}^{-1} \text{ cm}^{-2}$)	T_{in} (keV)	Disk Norm (10^{-3})	χ^2_{ν} /d.o.f. or (W-stat)	Disk Flux ($10^{-14} \text{ erg s}^{-1} \text{ cm}^{-2}$)
352 (2000-07-29)	2.4 (± 0.4)	1.23/28	3.4 (± 0.9)	0.4 (± 0.1)	109.0 ($^{+163.4}_{-69.4}$)	1.26/28	2.5 (± 0.05)
2707 (2002-07-06)	2.1 (± 0.2)	1.09/59	2.7 (± 0.5)	0.6 (± 0.1)	10.1 (± 1.1)	0.89/59	2.2 (± 0.4)
3717 (2002-07-05)	1.5 (± 0.7)	0.42/14	6.2 ($^{+3.8}_{-2.3}$)	1.1 ($^{+2.8}_{-0.8}$)	≤ 1.5	0.51/14	4.3 ($^{+6.2}_{-1.6}$)
5826 (2005-03-03)	1.0 (± 0.3)	2.46/45	3.6 (± 0.7)	2.1 ($^{+1.8}_{-0.6}$)	≤ 0.2	2.34/45	3.2 (± 0.7)
5827 (2005-05-05)	2.3 (± 0.2)	0.80/60	3.6 (± 0.5)	0.8 (± 0.2)	4.8 ($^{+5.8}_{-2.6}$)	0.86/60	2.8 (± 0.4)
5828 (2005-11-17)	2.3 ($^{+1.9}_{-1.6}$)	0.64/10	2.3 ($^{+1.6}_{-1.0}$)	1.2 ($^{+1.2}_{-0.4}$)	≤ 4.7	(126.98/122)	2.9 ($^{+1.0}_{-0.9}$)
6186 (2005-01-31)	†	†	≤ 3.2	†	†	†	†
7210 (2005-11-16)	3.0 ($^{+1.0}_{-0.8}$)	0.183/8	3.7 ($^{+1.4}_{-1.2}$)	0.5	≤ 38.9	0.37/8	2.5 (± 0.8)
7211 (2005-11-16)	1.5 (± 0.9)	(81.81/70)	3.8 ($^{+2.3}_{-1.6}$)	-	-	-	-
18781 (2016-02-24)	2.7 (± 0.8)	1.12/19	3.6 (± 1.0)	0.7 ($^{+0.6}_{-0.4}$)	≤ 7.0	1.42/19	2.4 (± 0.8)
18782 (2016-02-26)	2.8 (± 0.8)	1.49/12	2.9 (± 1.0)	0.5 ($^{+0.3}_{-0.2}$)	≤ 22.4	2.0 (± 0.7)	-
18783 (2016-04-20)	1.6 ($^{+1.1}_{-0.6}$)	(106.96/111)	2.2 ($^{+1.4}_{-0.9}$)	-	-	-	-
18836 (2016-04-28)	2.4 ($^{+0.8}_{-0.9}$)	1.34/12	3.4 (± 1.0)	0.5 ($^{+1.2}_{-0.3}$)	≤ 15.3	1.63/12	2.2 (± 0.7)
18838 (2016-05-28)	2.9 (± 0.7)	0.64/21	2.3 (± 0.7)	0.4 ($^{+0.2}_{-0.1}$)	≤ 96.7	0.61/21	1.8 (± 0.6)
18856 (2016-06-12)	1.9 ($^{+1.0}_{-2.1}$)	(104.28/106)	2.1 (± 1.2)	-	-	-	-

Table 7. *Chandra* Fit Parameters and Fluxes (0.5–8 keV) for spectral best fit single-component models, `tbabs*pegpwlw` and `tbabs*diskbb` for M87-GCULX1. Hydrogen column density (N_H) frozen to $2.54 \times 10^{20} \text{cm}^{-2}$. Lower count observations fit with W-stat have their statistics presented in parentheses. All fluxes shown are unabsorbed. Values marked with - were detections but could not be fit with the `diskbb` model.

M87-GCULX1							
ObsID (Date)	TBABS*PEGPWLW			TBABS*DISKBB			
	Γ	χ^2_{ν} /d.o.f. or (W-stat)	PL Flux ($10^{-14} \text{ erg s}^{-1} \text{ cm}^{-2}$)	T_{in} (keV)	Disk Norm (10^{-3})	χ^2_{ν} /d.o.f. or (W-stat)	Disk Flux ($10^{-14} \text{ erg s}^{-1} \text{ cm}^{-2}$)
241 (2000-07-17)	3.0 ($^{+0.9}_{-0.7}$)	(21.40/27)	4.2 ($^{+1.6}_{-1.3}$)	0.4 ($^{+0.2}_{-0.1}$)	101.0 ($^{+656.1}_{-110.4}$)	(23.44/27)	3.4 ($^{+1.3}_{-1.1}$)
352 (2000-07-29)	1.8 (± 0.1)	1.74/22	7.5 (± 1.1)	0.6 (± 0.1)	20.9 ($^{+12.1}_{-7.8}$)	0.90/22	5.0 (± 0.6)
2707 (2002-07-06)	2.1 (± 0.1)	2.42/43	4.9 (± 0.4)	0.6 (± 0.1)	19.7 ($^{+10.3}_{-6.6}$)	3.10/43	3.8 (± 0.3)
3717 (2002-07-05)	1.9 (± 0.3)	0.69/8	5.7 ($^{+1.3}_{-1.1}$)	0.7 ($^{+0.2}_{-0.1}$)	11.3 (± 89.0)	0.76/8	4.0 (± 0.8)
5826 (2005-03-03)	2.2 (± 0.3)	1.51/11	4.5 (± 0.6)	0.7 (± 0.2)	7.4 ($^{+11.6}_{-4.4}$)	2.06/11	3.3 (± 0.5)
5827 (2005-05-05)	1.9 (± 0.1)	1.40/32	4.5 (± 0.4)	0.9 (± 0.1)	3.2 (± 1.8)	1.57/32	3.9 (± 0.4)
5828 (2005-11-17)	2.7 ($^{+0.8}_{-0.6}$)	0.85/8	5.0 (± 0.9)	0.4 ($^{+0.3}_{-0.1}$)	≤ 54.3	3.32/8	2.8 (± 0.6)
6186 (2005-01-31)	2.1 (± 0.2)	1.33/12	4.0 (± 0.8)	0.8 (± 0.2)	6.1 ($^{+6.9}_{-3.1}$)	1.36/12	4.5 (± 0.6)
7210 (2005-11-16)	2.3 (± 0.7)	2.32/6	5.8 ($^{+1.5}_{-1.1}$)	0.6 ($^{+0.3}_{-0.2}$)	≤ 13.8	3.50/6	3.6 ($^{+0.9}_{-0.7}$)
7211 (2005-11-16)	2.3 (± 0.4)	(30.99/63)	5.3 (± 1.1)	0.8 (± 0.3)	6.0 (± 4.3)	(39.82/63)	3.6 (± 1.0)
18781 (2016-02-24)	2.6 (± 0.3)	2.09/12	4.4 (± 0.8)	0.5 (± 0.1)	35.4 ($^{+46.7}_{-20.0}$)	2.08/12	4.2 (± 0.6)
18782 (2016-02-26)	2.4 (± 0.3)	1.13/9	4.7 (± 0.9)	0.6 (± 0.1)	19.7 ($^{+32.8}_{-21.1}$)	1.67/9	4.2 (± 0.6)

erg/s. J04-GCULX shows some evidence of variability, as it was observed bright in all observations except for being an upper limit/non-detection in ObsID 6186 (2005-01-31). M87-GCULX3 was initially observed as an upper limit with a luminosity below 2×10^{38} erg/s in ObsID 352 (2000-07-29), and brightening in subsequent observations. M87-GCULX2 is observed bright until ObsID 18782 (2016-02-26) and fades in ObsID 18783 (2016-04-20), but rebrightens for ObsIDs 18836–18856 (2016-04-28, 2016-05-28, 2016-06-12).

3.4 Comparison of X-ray and Optical Parameters

We use the K-S test⁶ to compare magnitudes to the greater cluster population (as identified by (Jordán et al. 2009)). The K-S statistic probability is 0.57 (p value=0.006), which implies that the magnitudes of the host cluster population and the overall cluster population are very different. The Anderson-Darling test statistic is 7.00 (significance level=0.001), which is in agreement with the result of the K-S test. Therefore, the presences of ULXs in the clusters are not

⁶ https://docs.scipy.org/doc/scipy-0.14.0/reference/generated/scipy.stats.ks_2samp.html

Table 8. *Chandra* Fit Parameters and Fluxes (0.5-8 keV) for spectral best fit single-component models, `tbabs*pegpwr1w` and `tbabs*diskbb` for M87-GCULX2. Hydrogen column density (N_H) frozen to $2.54 \times 10^{20} \text{cm}^{-2}$. Lower count observations fit with W-stat have their statistics presented in parentheses. All fluxes shown are unabsorbed. Values marked with † are upper-limits based on the count rate of a non-detection (see Table 11), values marked with - were detections but could not be fit with the `diskbb` model.

M87-GCULX2							
ObsID (Date)	TBABS*PEGPWR1W			TBABS*DISKBB			
	Γ	$\chi^2_{\nu}/\text{d.o.f.}$ or (W-stat)	PL Flux ($10^{-14} \text{ erg s}^{-1} \text{ cm}^{-2}$)	T_{in} (keV)	Disk Norm (10^{-3})	$\chi^2_{\nu}/\text{d.o.f.}$ or (W-stat)	Disk Flux ($10^{-14} \text{ erg s}^{-1} \text{ cm}^{-2}$)
352 (2000-07-29)	1.7 ($^{+0.8}_{-0.7}$)	0.90/8	1.2 (± 0.6)	1.0 ($^{+2.0}_{-0.6}$)	≤ 0.5	0.98/8	1.0 (± 0.6)
2707 (2002-07-06)	1.6 (± 0.4)	1.07/23	1.6 (± 0.5)	1.0 ($^{+0.9}_{-0.4}$)	≤ 0.5	1.11/23	1.1 (± 0.4)
3717 (2002-07-05)	2.1 ($^{+1.9}_{-1.1}$)	2.29/4	1.5 ($^{+1.2}_{-0.8}$)	-	-	-	-
5826 (2005-03-03)	1.6 (± 0.4)	1.37/21	2.1 (± 0.5)	1.5 ($^{+1.1}_{-0.5}$)	≤ 0.2	1.57/21	1.8 (± 0.4)
5827 (2005-05-05)	1.3 (± 0.2)	1.12/30	3.1 (± 0.5)	1.4 ($^{+0.5}_{-0.3}$)	0.3 (± 0.2)	0.94/30	2.5 (± 0.5)
5828 (2005-11-17)	0.9 ($^{+0.6}_{-0.8}$)	(58.75/80)	2.2 ($^{+1.0}_{-0.8}$)	-	-	-	-
6186 (2005-01-31)	1.6 (± 0.6)	0.24/8	2.4 (± 0.7)	1.6 ($^{+1.7}_{-0.6}$)	≤ 0.2	0.28/8	2.1 (± 0.7)
18781 (2016-02-24)	0.9 ($^{+0.6}_{-0.8}$)	(83.23/104)	2.6 ($^{+1.5}_{-1.8}$)	-	-	-	-
18782 (2016-02-26)	1.2 (± 0.6)	(81.61/96)	3.3 ($^{+1.4}_{-1.0}$)	-	-	-	-
18783 (2016-04-20)	†	†	≤ 2.1	†	†	†	†
18836 (2016-04-28)	1.9 (± 0.7)	(69.16/65)	3.1 (± 1.1)	1.5 ($^{+3.3}_{-0.7}$)	≤ 0.3	(72.76/65)	1.5 ($^{+0.8}_{-0.6}$)
18838 (2016-05-28)	1.1 (± 1.0)	(55.78/77)	1.9 ($^{+1.2}_{-0.9}$)	-	-	-	-
18856 (2016-06-12)	1.9 (± 0.7)	(54.44/77)	2.1 ($^{+1.0}_{-0.8}$)	1.1 ($^{+1.8}_{-0.5}$)	≤ 0.7	(55.78/77)	1.8 ($^{+1.0}_{-0.7}$)

Table 9. *Chandra* Fit Parameters and Fluxes (0.5-8 keV) for spectral best fit single-component models, `tbabs*pegpwr1w` and `tbabs*diskbb` for M87-GCULX3. Hydrogen column density (N_H) frozen to $2.54 \times 10^{20} \text{cm}^{-2}$. Lower count observations fit with W-stat have their statistics presented in parentheses. All fluxes shown are unabsorbed. Values marked with † are upper-limits based on the count rate of a non-detection (see Table 11), values marked with - were detections but could not be fit with the `diskbb` model.

M87-GCULX3							
ObsID (Date)	TBABS*PEGPWR1W			TBABS*DISKBB			
	Γ	$\chi^2_{\nu}/\text{d.o.f.}$ or (W-stat)	PL Flux ($10^{-14} \text{ erg s}^{-1} \text{ cm}^{-2}$)	T_{in} (keV)	Disk Norm (10^{-3})	$\chi^2_{\nu}/\text{d.o.f.}$ or (W-stat)	Disk Flux ($10^{-14} \text{ erg s}^{-1} \text{ cm}^{-2}$)
352 (2000-07-29)	†	†	≤ 3.7	†	†	†	†
2707 (2002-07-06)	1.1 (± 0.4)	(156.64/173)	1.9 (± 0.5)	-	-	-	-
3717 (2002-07-05)	1.9 ($^{+1.0}_{-0.9}$)	(49.64/69)	1.2 ($^{+1.1}_{-0.7}$)	0.6 ($^{+1.0}_{-0.3}$)	≤ 3.9	(48.73/69)	0.8 ($^{+0.7}_{-0.4}$)
5826 (2005-03-03)	1.6 (± 0.2)	(191.14/203)	3.4 (± 0.5)	-	-	-	-
5827 (2005-05-05)	1.3 (± 0.2)	(183.55/243)	4.4 (± 0.5)	2.1 ($^{+0.7}_{-0.4}$)	0.1 (± 0.1)	(187.27/243)	4.1 (± 0.5)
5828 (2005-11-17)	1.7 (± 0.4)	(77.52/97)	3.8 ($^{+1.0}_{-0.9}$)	1.3 ($^{+0.5}_{-0.3}$)	≤ 0.7	(76.02/97)	3.3 (± 0.9)
6186 (2005-01-31)	1.3 (± 0.4)	(126/17/146)	4.0 (± 1.0)	-	-	-	-
7210 (2005-11-16)	1.8 (± 0.5)	(78.90/92)	3.0 ($^{+1.0}_{-0.8}$)	-	-	-	-
7211 (2005-11-16)	1.4 (± 0.5)	(47.41/76)	5.4 ($^{+2.8}_{-1.5}$)	1.8 ($^{+2.8}_{-0.6}$)	≤ 0.3	(49.22/76)	5.0 ($^{+2.1}_{-1.5}$)
18781 (2016-02-24)	2.0 (± 0.7)	(71.05/84)	1.9 (± 0.8)	0.9 ($^{+0.9}_{-0.3}$)	≤ 1.2	(72.95/84)	1.5 ($^{+0.7}_{-0.5}$)
18782 (2016-02-26)	1.4 (± 0.7)	(74.25/76)	1.8 ($^{+0.8}_{-0.6}$)	-	-	-	-
18836 (2016-04-28)	1.2 ($^{+0.6}_{-0.7}$)	(80.19/72)	2.0 ($^{+0.9}_{-0.7}$)	-	-	-	-
18838 (2016-05-28)	1.3 (± 0.6)	(80.04/93)	2.4 ($^{+0.9}_{-0.7}$)	-	-	-	-
18856 (2016-06-12)	1.2 ($^{+0.6}_{-0.8}$)	(51.41/62)	2.0 ($^{+0.8}_{-0.6}$)	-	-	-	-

evenly distributed across different cluster parameters, but tend to reside in the most luminous (and also the more massive) clusters.

A K-S test of the metallicity of the ULX hosting clusters compared to the clusters identified in (Jordán et al. 2009) gave a probability of 0.38 (p value=0.15). The Anderson-Darling test statistic is 0.68, with a significance level equal to 0.17. These numbers indicate that one cannot meaningfully separate the ULX hosting clusters from the rest of the sample based on their color. Previous work by Kundu et al. 2002; Sarazin et al. 2003 have indicated that metal rich globular clusters are three times as likely to host low mass X-ray binaries. Many subsequent analyses have firmly established

this correlation for X-ray binaries in GCs. But this data set strongly suggests that the affinity for metal rich GCs does not extend to the most luminous subset of XRBs which make up the ULX population. This tentative disagreement may be due to the physics behind the formation and evolution of ULX systems in globular clusters compared to the less luminous X-ray binaries, although it is worth noting that the majority of these clusters are not spectroscopically confirmed, and that SC302 is also in the mass range of a stripped nucleus (see Section 3.5).

Figure 7 shows the best fit X-ray parameters for both models plotted against the absolute z magnitude and color ($g - z$) of the

Table 10. *Chandra* Fit Parameters and Fluxes (0.5-8 keV) for spectral best fit single-component models, `tbabs*pegpwlw` and `tbabs*diskbb` for M87-GCULX4. Hydrogen column density (N_H) frozen to $2.54 \times 10^{20} \text{cm}^{-2}$. Lower count observations fit with W-stat have their statistics presented in parentheses. All fluxes shown are unabsorbed. Values marked with - were detections but could not be fit with the `diskbb` model.

M87-GCULX4							
ObsID (Date)	TBABS*PEGPWLW			TBABS*DISKBB			
	Γ	$\chi^2_v/\text{d.o.f.}$ or (W-stat)	PL Flux ($10^{-14} \text{erg s}^{-1} \text{cm}^{-2}$)	T_{in} (keV)	Disk Norm (10^{-3})	$\chi^2_v/\text{d.o.f.}$ or (W-stat)	Disk Flux ($10^{-14} \text{erg s}^{-1} \text{cm}^{-2}$)
352 (2000-07-29)	1.1 (± 0.41)	(46.37/71)	2.5 ($^{+1.1}_{-0.8}$)	-	-	-	-
2707 (2002-07-06)	1.3 (± 0.3)	1.13/18	2.1 (± 0.6)	1.5 ($^{+1.2}_{-0.5}$)	≤ 0.2	1.22/18	1.6 (± 0.6)
5826 (2005-03-03)	1.6 (± 0.5)	1.07/7	1.3 (± 0.3)	1.7 ($^{+1.7}_{-0.6}$)	≤ 0.1	1.57/7	1.2 (± 0.4)
5827 (2005-05-05)	1.2 (± 0.4)	0.69/7	1.7 (± 0.5)	2.1 ($^{+4.6}_{-0.8}$)	≤ 0.1	0.72/7	1.5 (± 0.6)
5828 (2005-11-17)	2.1 ($^{+0.7}_{-0.6}$)	(41.79/43)	1.7 ($^{+0.6}_{-0.5}$)	1.0 ($^{+0.7}_{-0.4}$)	≤ 0.8	(43.85/43)	1.3 ($^{+0.6}_{-0.4}$)
7210 (2005-11-16)	2.0 ($^{+0.7}_{-0.6}$)	(33.68/31)	1.5 ($^{+0.7}_{-0.5}$)	1.0 ($^{+0.9}_{-0.4}$)	≤ 0.7	(35.77/31)	1.3 ($^{+0.6}_{-0.5}$)

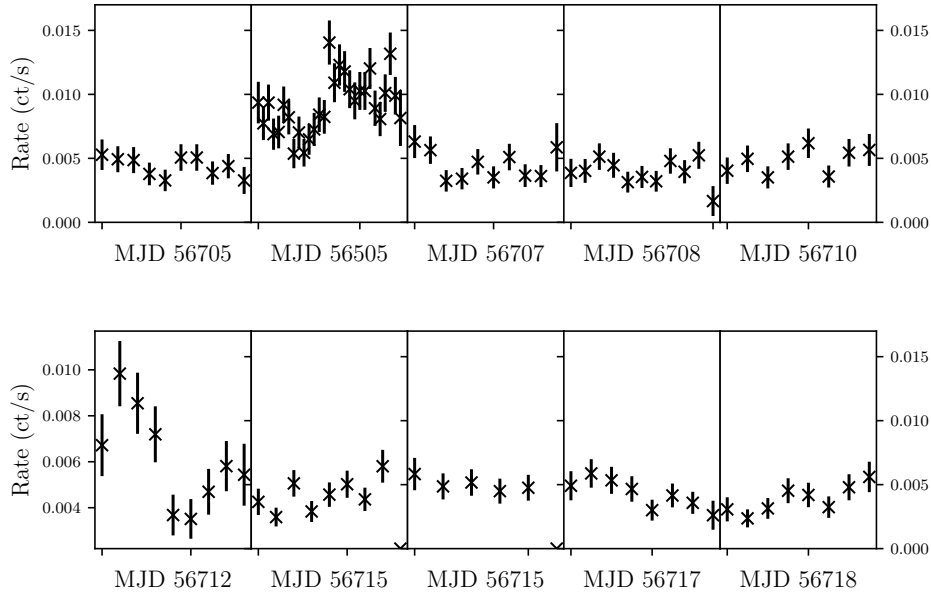


Figure 3. Background-subtracted light curves from SC302 across all observations, binned by 5ks in the 0.3-10 keV band. The source shows significant variability in two of the observations, and is one of the few GCULXs to do so.

Source	ObsID	Count Rate (ct/s)	Flux Upper Limits $\text{erg s}^{-1} \text{cm}^{-2}$
L18-GCULX	352	4.1×10^{-3}	2.09×10^{-14}
M87-GCULX3	352	4.7×10^{-3}	3.71×10^{-14}
L18-GCULX	3717	3.9×10^{-3}	1.99×10^{-14}
J04-GCULX	6186	5.11×10^{-3}	3.23×10^{-14}
L18-GCULX	11783	1.6×10^{-3}	1.06×10^{-14}
M87-GCULX2	18783	1.8×10^{-3}	2.14×10^{-14}

Table 11. Background subtracted upper limit count rates and upper flux limit estimates for GCULXs in the 0.5-8keV band.

source's cluster companions. The color distribution of the M87 cluster hosts is more concentrated, and neither very red, nor very

Table 12. RMS values for individual observations of SC302.

ObsID	RMS
15179	0.32 (± 0.11)
15180	0.24 (± 0.08)
16590	0.37 (± 0.13)
16591	0.39 (± 0.16)

blue, but previous ULX hosting clusters have been observed to be both extremely red and extremely blue. This suggests that the M87 sources are more typical hosts of GC ULXs, with RZ2109, GCU7 and GCU8 being the outliers in this strange population of bright X-ray sources.

A study of M31's globular clusters by [Trudolyubov & Priedhorsky 2004](#) show that the most luminous X-ray sources ($\sim 10^{38}$

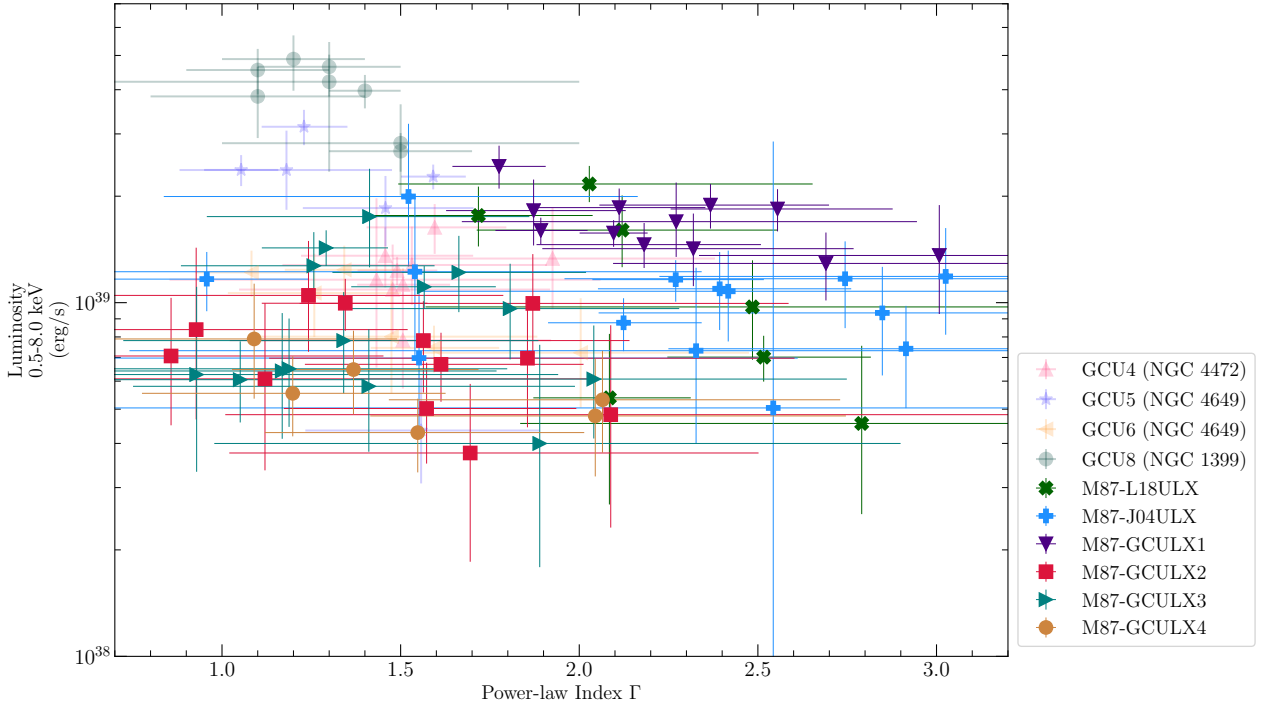


Figure 4. L_X versus Γ for M87's newly discovered GC ULX population compared to fit parameters for other known GC ULXs (Dage et al. 2019a).

erg/s) are associated with the most metal poor clusters. However, this does not seem to be true for M87's ultraluminous population, as the clusters values for $(g-z)$ all ranged above 1.0—although other GCULXs such as RZ2109 have $(g-z)$ values below 1.0. Kundu et al. 2007 suggest that for most GCs with a high L_X , that luminosity is coming in majority from only one low mass X-ray binary (LMXB) source, and that the only clusters that are likely to host many bright LMXB sources are the very metal rich clusters, which M87's ULX population also does not fall into.

3.5 Summary of Sources

In the following subsections we present a summary and discussion of the seven sources analysed in this paper.

3.5.1 CXOUJ122959.82123812.33 (SC302)

SC302 is in the Virgo Cold Front, and 19' from M87's galaxy centre. It is the only spectroscopically confirmed GC in this sample of GC hosts, with $z=19.76$ and $(g-z)=1.01$. However, the cluster mass is $3.33 \times 10^6 M_\odot$, which is in the range of either a GC or stripped nucleus. This source is the brightest optical cluster in this sample, and also the most metal poor (although it is not as metal poor as some of the other known GCULXs such as RZ2109). The source's best-fit power-law index based on the stacked spectra is $\Gamma=2.07$ and the DISKBB $kT=0.92$ keV. χ^2 statistics of the deep spectrum suggest that this source is better fit by the DISKBB model.

While there are many observations of this source, they have been taken over approximately one year in span, so we do not have a good idea of the long-term variability of this source; however, it shows curious short-term variability on the scale of hours from its extracted lightcurves. It varies both in L_X and in its spectral parameter in a similar fashion to GCU1 in NGC 4472 (Maccarone

et al. 2011; Dage et al. 2019a). It is also the brightest X-ray source in this sample, with its peak X-ray luminosity reaching close to 4×10^{39} erg/s.

3.5.2 CXOUJ123054.97+122438.51 (L18-GCULX)

L18-GCULX's host cluster is both the faintest cluster and most metal rich in the sample, with $z=22.58$, $(g-z)=1.70$, and cluster mass $2.53 \times 10^5 M_\odot$. $\Gamma=2.03$ (± 0.11) and $kT=0.81$ (± 0.09) keV. This source shows a strong variation in L_X over the course of many observations, but little variability within an observation.

3.5.3 CXOUJ123049.24+122334.52 (J04-GCULX)

J04-GCULX is the closest source to the galaxy centre, and the GC has $z=21.68$ and $(g-z)=1.08$, with the cluster mass $5.70 \times 10^5 M_\odot$. Overall, the source has a softer power-law index. The best-fit spectral parameters of the stacked spectrum are $\Gamma=2.21$ (± 0.09) and $kT=0.74$ (± 0.07) keV. The fit statistics of the stacked spectrum do not delineate between either model. Note that the high background near the galaxy center affected background subtraction of the source's spectrum, specifically with the lower counts.

Long-term, the source appears to vary moderately near 1×10^{39} erg/s, with some brighter and fainter excursions over the full dataset. However, within an observation, shows no clear variability (Foster et al. 2013), see Appendix A.

3.5.4 CXOUJ123047.12+122416.06 (M87-GCULX1)

M87-GCULX was matched to two possible host clusters which have $z=21.93$ (cluster mass = $5.04 \times 10^5 M_\odot$) or 22.55 (estimated cluster mass = $2.60 \times 10^5 M_\odot$) and $(g-z)=1.05$ or 1.61. Its stacked X-ray spectrum appears to be better fit by `tbabs*(diskbb+pegpwr1w)`,

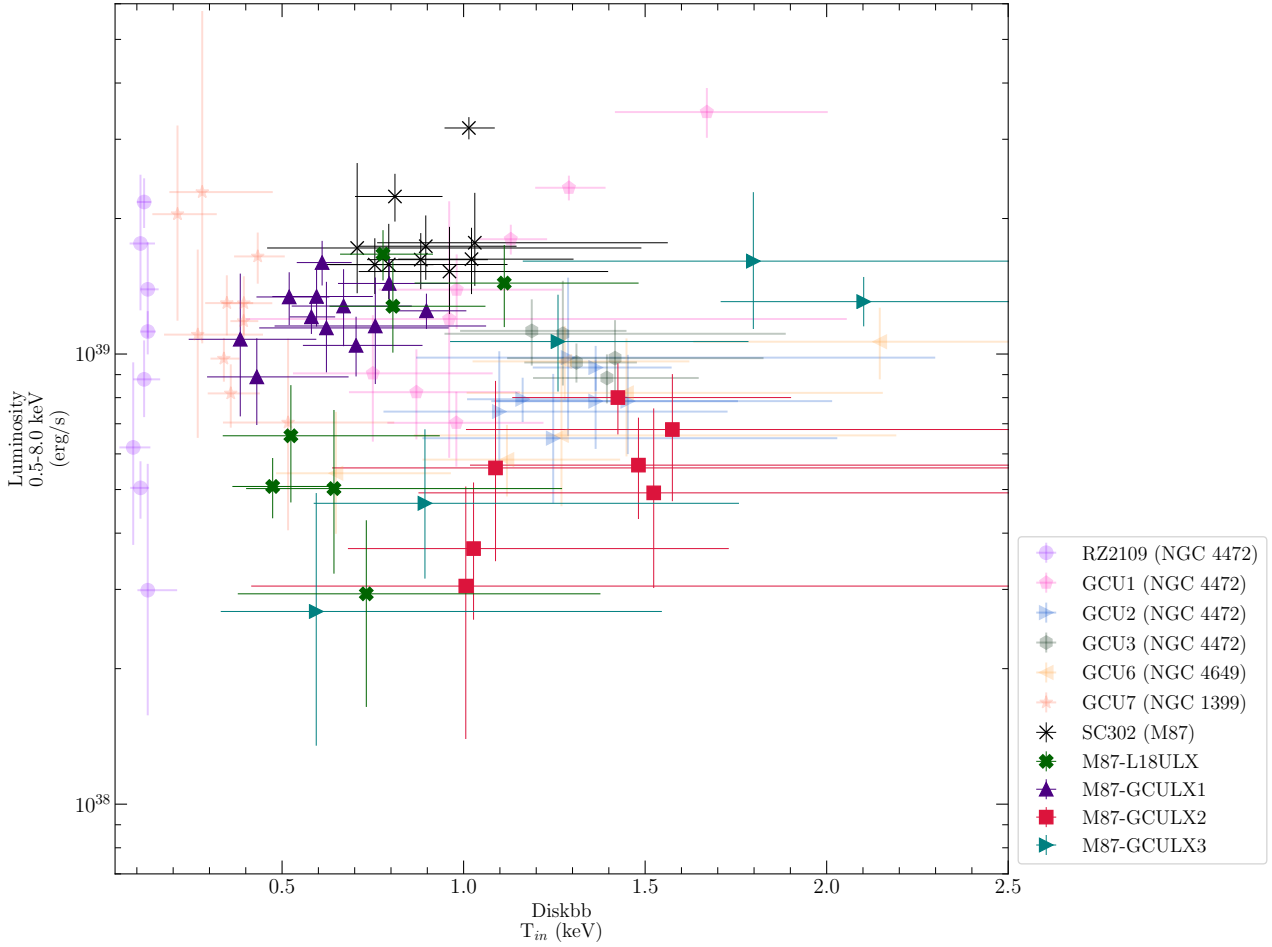


Figure 5. L_X versus T_{in} for M87’s newly discovered GC ULX population compared to fit parameters for other known GC ULXs (Dage et al. 2019a).

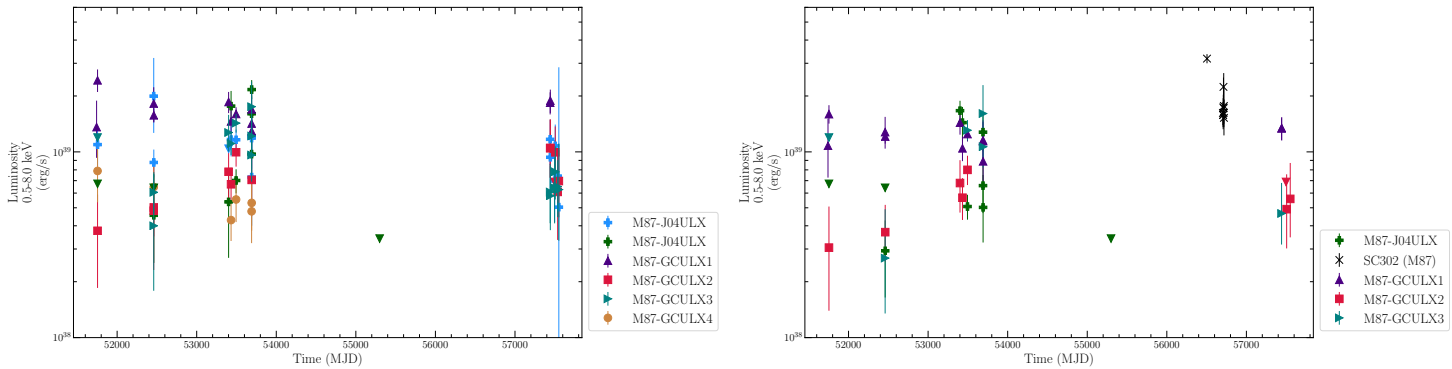


Figure 6. L_X versus MJD for M87’s newly discovered GC ULX population, with L_X calculations based off of best fit PEGPWLW fluxes (left) and best fit DISKBB fluxes (right).

with $kT \sim 0.56$ keV and $\Gamma \sim 1.95$. However, we were unable to fit the individual observations with the two component model without either of the components having large uncertainties consistent with zero.

Long-term, over the course of the observations, its average X-ray luminosity tends to vary between $1\text{--}3 \times 10^{39}$ erg/s. Within an observation, similar to J04-GCULX, it also shows no clear variability within the observations (Foster et al. 2013), see Appendix A.

3.5.5 *CXOUJ123050.12+122301.14* (M87-GCULX2)

The properties of the host cluster of M87-GCULX2 are $z=20.49$, $(g-z)=1.29$, and an estimated cluster mass of $1.73 \times 10^6 M_\odot$. There was no clear delineation between models for this source. The best-fit parameters of the stacked spectrum are $\Gamma = 1.52(\pm 0.11)$ and $kT = 1.44 (\pm 0.21)$. The fit statistics of the stacked spectrum do not delineate between either model. Note that the high background near

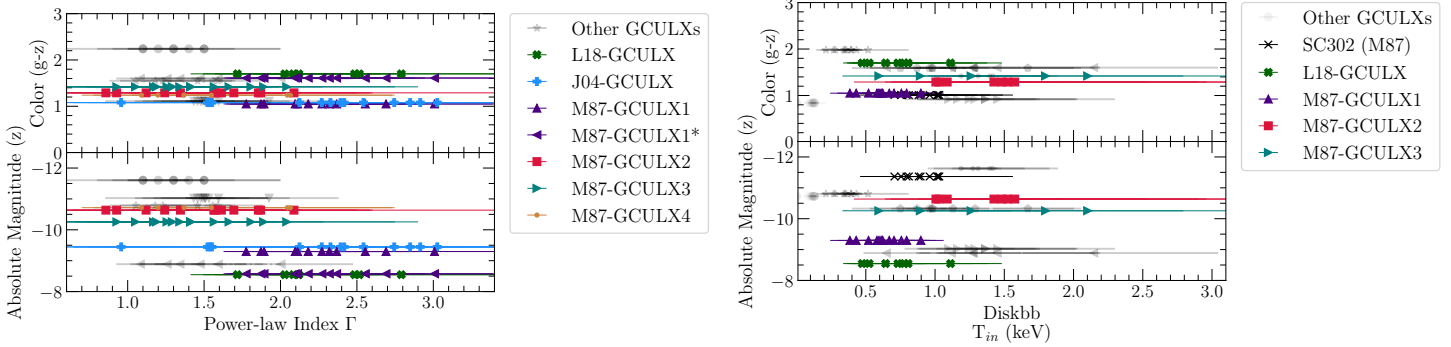


Figure 7. Color and magnitude versus best fit power-law index (left) and kT (right) for M87 GC ULXs compared to previous GC ULXs Dage et al. 2019a.

the galaxy center affected background subtraction of the source’s spectrum, specifically with the lower counts.

This source shows interesting variability. It is one of the fainter ultraluminous X-ray sources, only reaching about 10^{39} erg/s in a few observations. It also shows variability on timescales of \sim days; it was observed near 10^{39} erg/s on 2016-02-26, but was a non-detection on 2016-04-20, but 8 days later in the next observation, it reached 10^{39} erg/s again, and remained bright in the following observations. It is quite likely that the source shows high amplitude variability, which could be confirmed by a monitoring campaign on this region.

3.5.6 CXOUJ123049.97+122400.11 (M87-GCULX3)

M87-GCULX3’s cluster has optical properties of $z=20.87$ and $(g-z)=1.42$. The estimated cluster mass is $1.22 \times 10^6 M_{\odot}$. The X-ray spectrum of this source needed to be binned by 1 and fit with W-statistics in all observations, and is one of the faintest X-ray sources in this sample, only reaching about 10^{39} erg/s in one observation when fit with `tbabs*pegpwlw`, so the source is not even securely classified as ultraluminous. Its best fit spectral parameters based on the stacked spectrum are $\Gamma=1.36 (\pm 0.09)$ and $kT= 1.90 (\pm 0.28)$ keV. The source shows no clear short term variability, but these fits are not well constrained in the individual observations due to the faintness of the source. The fit statistics of the stacked spectrum do not delineate between either model.

Unlike the rest of the sources in this sample, M87-GCULX3 was below 10^{39} erg/s in almost all of the observations. It likely has a different physical mechanism than the rest of the sources in this sample, and may possibly be comparable to Z track neutron star sources which show a roughly similar luminosity variability (e.g. Nikolaeva et al. 2018). Some candidate Z sources have been identified in globular clusters such as Terzan-5 and GCs in M31 (Barnard et al. 2003; Linares et al. 2012), as well as extragalactic globular clusters associated with NGC 3115 (although none of these were observed to reach 10^{39} erg/s) (Lin et al. 2015).

In a study of globular cluster X-ray sources in NGC 3379, Brassington et al. 2010 found a source with X-ray luminosities on the order of 10^{38} erg/s which reached close to 10^{39} erg/s in an observation, and was best fit with $\Gamma = 1.85$, which may also be similar to M87-GCULX3.

3.5.7 CXOUJ123041.77+122440.16 (M87-GCULX4)

M87-GCULX4’s host cluster is $z=20.41$, $(g-z)=1.24$ and an estimated cluster mass of $1.86 \times 10^6 M_{\odot}$. This source is one of the hardest in the sample, with $\Gamma= 1.37 (\pm 0.15)$ $kT= 1.86 (^{+0.56}_{-0.38})$, based

on the stacked spectrum, with the fit statistics favouring the power-law model as the best fit model. This source’s spectrum was also affected due to the the high background near the galaxy center.

The variability in this source is interesting in the long-term, as it was observed turning on in the first two observations, and rising to just above 10^{39} erg/s for many of the early observations. The cluster of observations shows the source clustered just below 10^{39} erg/s. The lightcurves do not appear to show any short term variability.

4 CONCLUSIONS

GC ULXs comprise a very rare population, as the chance of an individual cluster hosting a ULX is very low, indeed. Previously, only 10 had been identified, 3 associated with NGC 1399 (one of which “turned off” in 2003 and has not been observed above the observation detection limit since) (Shih et al. 2010; Irwin et al. 2010; Dage et al. 2019a), two associated with NGC 4649 (Roberts et al. 2012; Dage et al. 2019a), and five associated with NGC 4472 (Maccarone et al. 2007, 2011; Dage et al. 2019a).

A new search of M87’s beautiful GC system revealed seven new GC ULX sources, almost doubling the known sample, which is not surprising, as the size of M87’s globular cluster system means that the size of the cluster sample that has been searched for ULXs has roughly doubled as well. One of these sources, SC302, is a spectroscopically confirmed GC with a measured radial velocity (Strader et al in prep, see also Caldwell et al. 2014), while the rest are photometrically selected GCs from surveys by (Jordán et al. 2009; Oldham & Auger 2016). We recommend detailed optical follow-up on these sources in the future, as the sources studied in Dage et al. 2019a are postulated to show a correlation between the presence of optical emission lines and the X-ray spectral behaviour of the source. A high-resolution spectrum would not only confirm the globular cluster nature of the host sources, but place upper limits on any optical emission coming from the source.

Many of these newly discovered sources in M87 show striking variability over the 16 years that they have been monitored, in some cases showing order of magnitude variability. However, many of these sources are also remarkably steady over the timescales probed as well, which is similar to the sample studied in Dage et al. 2019a. M87-GCULX2 is especially interesting, as it seems to vary strongly between sub-Eddington and super-Eddington timescales at least on the scale of months.

None of the sources in the M87 sample rose above 4×10^{39} erg/s, and the overall L_X of the previously studied sample suggests

that these sources also do not rise above 4×10^{39} erg/s over a total observation, with the exception of GCU8 in NGC 1399.

Interestingly, the optical properties of the cluster (i.e. colour and magnitude) again do not seem to show any correlation with the X-ray temporal or spectral properties. In fact the results of this study only serve to highlight how different the very soft sources such as RZ2109 (NGC 4472) and GCU7 (NGC 1399), or the very hard source GCU8 (NGC 1399) are different from the rest of the GC ULX population.

We postulate that the accretors of these systems are most likely black holes. While some ULXs in young, star-forming galaxies have been identified to have neutron star primaries (e.g. Song et al. 2020), the nature of these sources cannot inform on the nature of the accretors in the globular cluster systems due to a number of key environmental and phenomenological differences. Namely, the X-ray binaries in the star-forming regions of galaxies have massive, hydrogen rich donor stars (Gladstone et al. 2013), whereas only lower mass donor stars remain in the very much older globular cluster environment. The globular cluster binaries also face a vastly more dynamic and complicated evolutionary history, with the more massive cluster component likely having exchanged multiple companions throughout its lifetime due to preferential mass exchange (Spitzer 1987). Finally, the observational characteristics of the two populations differ greatly. The ULXs with neutron star primaries have all been observed at X-ray luminosities near 10^{40} erg/s (Bachetti et al. 2014), whereas the GC ULXs are observed between $1-4 \times 10^{39}$ erg/s. The spectra of the ULXs in star-forming regions typically consist of a soft component added to a hard component, or a broadened disk (Kaaret et al. 2017), yet with one exception the sources in this study were best fit by single-component models.

DATA AVAILABILITY STATEMENT

The X-ray data in this article is publicly available through the *Chandra* archive⁷.

ACKNOWLEDGEMENTS

We thank the referee, Jimmy Irwin, for a helpful report which improved the quality and presentation of the results in this paper. KCD, SEZ, and MBP acknowledge support from Chandra grant GO4-15089A. SEZ and MBP also acknowledge support from the NASA ADAP grant NNX15AI71G. JS acknowledges support from the Packard Foundation. KCD acknowledges Elias Aydi, Rufus Byrd, Chelsea Harris and Jimmy Irwin for their help. This research has made use of data obtained from the Chandra Data Archive and the Chandra Source Catalog. We also acknowledge use of NASA's Astrophysics Data System and Arxiv.

The following software and packages were used for analysis: CIAO, software provided by the Chandra X-ray Center (CXC), HEASOFT obtained from the High Energy Astrophysics Science Archive Research Center (HEASARC), a service of the Astrophysics Science Division at NASA/GSFC and of the Smithsonian Astrophysical Observatory's High Energy Astrophysics Division, SAOImage DS9, developed by Smithsonian Astrophysical Observatory, NUMPY (van der Walt et al. 2011), and MATPLOTLIB (Hunter 2007).

REFERENCES

- Abbott B. P., et al., 2016, *ApJ*, **833**, L1
 Bachetti M., et al., 2014, *Nature*, **514**, 202
 Barnard R., Kolb U., Osborne J. P., 2003, *A&A*, **411**, 553
 Brassington N. J., et al., 2010, *ApJ*, **725**, 1805
 Brightman M., et al., 2018, *Nature Astronomy*, **2**, 312
 Brightman M., et al., 2019, arXiv e-prints, p. arXiv:1912.04431
 Caldwell N., Strader J., Romanowsky A. J., Brodie J. P., Moore B., Diemand J., Martizzi D., 2014, *ApJ*, **787**, L11
 Cash W., 1979, *ApJ*, **228**, 939
 Chomiuk L., Strader J., Maccarone T. J., Miller-Jones J. C. A., Heinke C., Noyola E., Seth A. C., Ransom S., 2013, *ApJ*, **777**, 69
 Dage K. C., Zepf S. E., Peacock M. B., Bahramian A., Noroozi O., Kundu A., Maccarone T. J., 2019a, *MNRAS*, **485**, 1694
 Dage K. C., et al., 2019b, *MNRAS*, **489**, 4783
 Dickey J. M., Lockman F. J., 1990, *ARA&A*, **28**, 215
 Fabbiano G., White N. E., 2006, *Compact stellar X-ray sources in normal galaxies*. Cambridge University Press, pp 475–506
 Fabricant D., Topka K., Harnden F. R. J., Gorenstein P., 1978, *ApJ*, **226**, L107
 Foster D. L., Charles P. A., Swartz D. A., Misra R., Stassun K. G., 2013, *MNRAS*, **432**, 1375
 Fruscione A., et al., 2006, in *Society of Photo-Optical Instrumentation Engineers (SPIE) Conference Series*. p. 62701V, doi:10.1117/12.671760
 Giersz M., Askar A., Wang L., Hypki A., Leveque A., Spurzem R., 2019, *MNRAS*, **487**, 2412
 Giesers B., et al., 2018, *MNRAS*, **475**, L15
 Giesers B., et al., 2019, *A&A*, **632**, A3
 Gladstone J. C., Copperwheat C., Heinke C. O., Roberts T. P., Cartwright T. F., Levan A. J., Goad M. R., 2013, *ApJS*, **206**, 14
 Harris W. E., 2009, *ApJ*, **699**, 254
 Hunter J. D., 2007, *Computing in Science and Engineering*, **9**, 90
 Irwin J. A., Athey A. E., Bregman J. N., 2003, *ApJ*, **587**, 356
 Irwin J. A., Brink T. G., Bregman J. N., Roberts T. P., 2010, *ApJ*, **712**, L1
 Irwin J. A., et al., 2016, *Nature*, **538**, 356
 Jithesh V., Anjana C., Misra R., 2020, arXiv e-prints, p. arXiv:2004.01796
 Jordán A., et al., 2004, *ApJ*, **613**, 279
 Jordán A., et al., 2009, *ApJS*, **180**, 54
 Kaaret P., Feng H., Roberts T. P., 2017, *ARA&A*, **55**, 303
 Kajava J. J. E., Poutanen J., 2009, *MNRAS*, **398**, 1450
 King A. R., 2008, *MNRAS*, **385**, L113
 Kremer K., Chatterjee S., Ye C. S., Rodriguez C. L., Rasio F. A., 2019, *ApJ*, **871**, 38
 Kundu A., Maccarone T. J., Zepf S. E., 2002, *ApJ*, **574**, L5
 Kundu A., Maccarone T. J., Zepf S. E., 2007, *ApJ*, **662**, 525
 Larsen S. S., 1999, *A&AS*, **139**, 393
 Lin D., et al., 2015, *ApJ*, **808**, 19
 Linares M., Altamirano D., Chakrabarty D., Cumming A., Keek L., 2012, *ApJ*, **748**, 82
 Luan L., et al., 2018, *ApJ*, **862**, 73
 Maccarone T. J., Kundu A., Zepf S. E., Rhode K. L., 2007, *Nature*, **445**, 183
 Maccarone T. J., Kundu A., Zepf S. E., Rhode K. L., 2011, *MNRAS*, **410**, 1655
 Macri L. M., et al., 1999, *ApJ*, **521**, 155
 Miller-Jones J. C. A., et al., 2015, *MNRAS*, **453**, 3918
 Mitsuda K., et al., 1984, *PASJ*, **36**, 741
 Nikolaeva S. M., Krivonos R. A., Sazonov S. Y., 2018, *Astronomy Letters*, **44**, 593
 Oldham L. J., Auger M. W., 2016, *MNRAS*, **455**, 820
 Peacock M. B., et al., 2012, *ApJ*, **759**, 126
 Roberts T. P., et al., 2012, *ApJ*, **760**, 135
 Rodriguez C. L., Zevin M., Amaro-Seoane P., Chatterjee S., Kremer K., Rasio F. A., Ye C. S., 2019, *Phys. Rev. D*, **100**, 043027
 Sarazin C. L., Kundu A., Irwin J. A., Sivakoff G. R., Blanton E. L., Randall S. W., 2003, *ApJ*, **595**, 743
 Shih I. C., Kundu A., Maccarone T. J., Zepf S. E., Joseph T. D., 2010, *ApJ*, **721**, 323

⁷ <https://cda.harvard.edu/chaser/>

- Shishkovsky L., et al., 2018, *ApJ*, **855**, 55
- Song X., Walton D. J., Lansbury G. B., Evans P. A., Fabian A. C., Earnshaw H., Roberts T. P., 2020, *MNRAS*, **491**, 1260
- Spitzer L., 1987, Dynamical evolution of globular clusters
- Steele M. M., Zepf S. E., Kundu A., Maccarone T. J., Rhode K. L., Salzer J. J., 2011, *ApJ*, **739**, 95
- Strader J., et al., 2011, *ApJS*, **197**, 33
- Strader J., Chomiuk L., Maccarone T. J., Miller-Jones J. C. A., Seth A. C., 2012, *Nature*, **490**, 71
- Taylor M. B., 2005, TOPCAT & STIL: Starlink Table/VOTable Processing Software. Astronomical Society of the Pacific, p. 29
- Trudolyubov S., Priedhorsky W., 2004, *ApJ*, **616**, 821
- Walton D. J., et al., 2018, *ApJ*, **856**, 128
- Zepf S. E., et al., 2008, *ApJ*, **683**, L139
- van der Walt S., Colbert S. C., Varoquaux G., 2011, *Computing in Science and Engineering*, **13**, 22

APPENDIX A: LIGHTCURVES

Lightcurves from the longest observations of L18-GCULX, J04-GCULX, M87-GCULX1, M87-GCULX2, M87-GCULX3, and M87-GCULX4, binned by 5ks in the 0.3-10keV band.

This paper has been typeset from a \TeX/L\AA\TeX file prepared by the author.

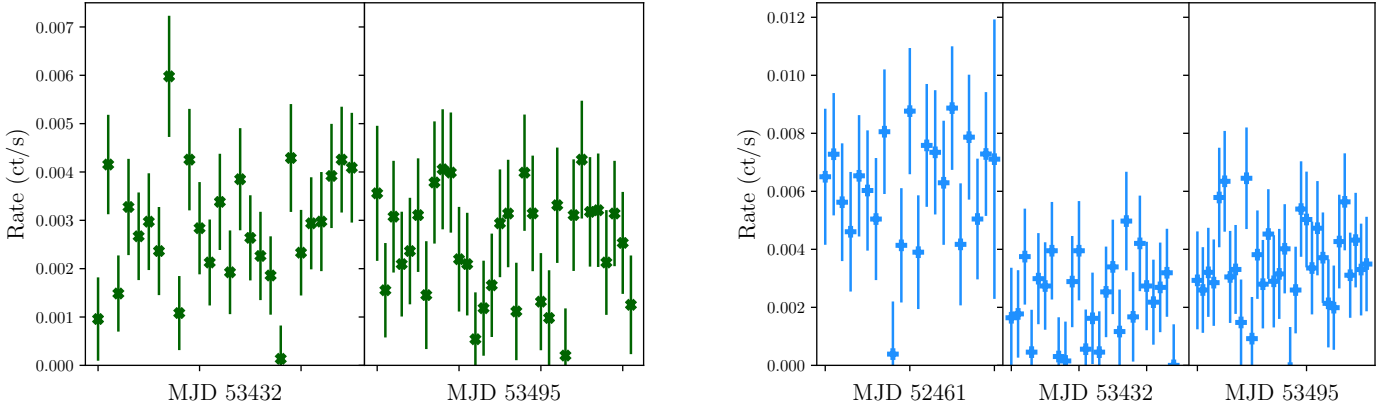


Figure A1. Lightcurves from L18-GCULX (left, ObsIDs 5826 and 5827) and J04-GCULX (right, ObsIDs 2707, 5826 and 5827), binned by 5ks.

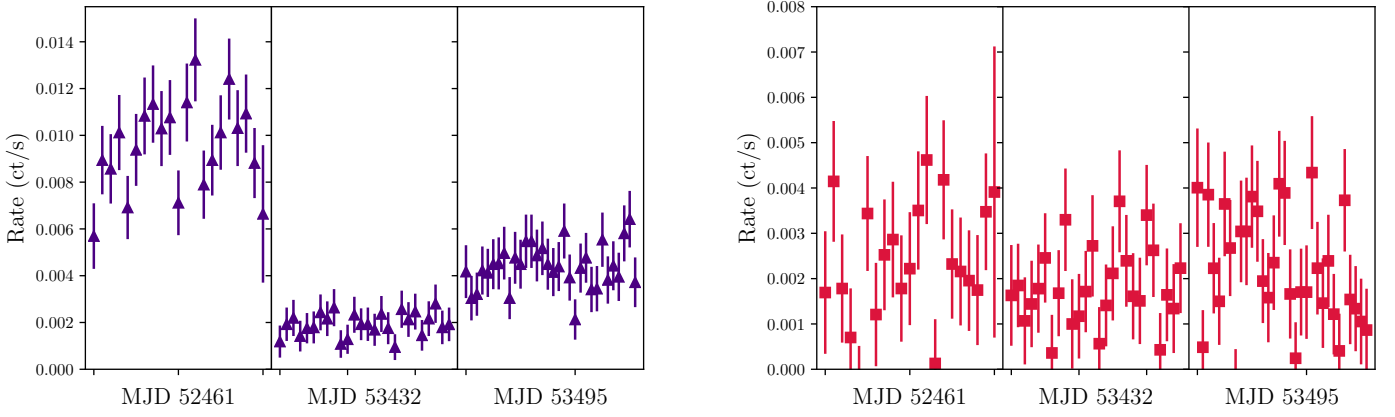


Figure A2. Lightcurves from M87-GCULX1 (left) and M87-GCULX2 (right) in ObsIDs 2707, 5826 and 5827, binned by 5ks.

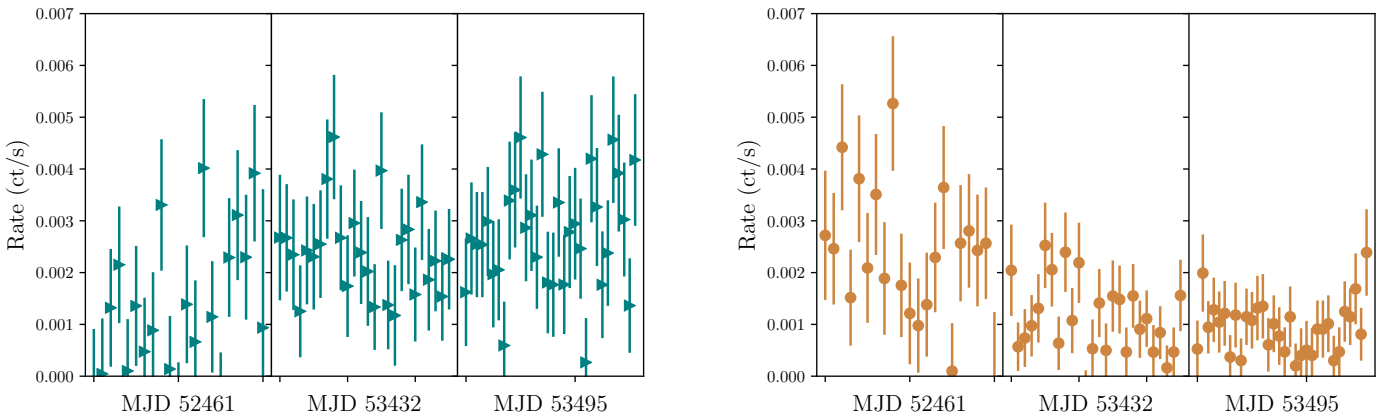


Figure A3. Lightcurves from M87-GCULX3 (right) M87-GCULX4 (left) in ObsIDs 2707, 5826 and 5827, binned by 5ks.